National University of
Science and Technology
POLITEHNICA
BUCHAREST

Doctoral School of Electronics, Telecommunications
and Information Technology

Decision no. 28 from 26.03.2024

Ph.D. THESIS SUMMARY

Eng. George BOLDEIU

SAW devices based on III - Nitrides for sensors applications and coupling of the surface acustic waves with spin waves

---

THESIS COMMITTEE

Prof. Dr. Eng. Ion MARGHESCU Univ. Politehnica din Bucureşti	President
CSI. Dr. Alexandru MÜLLER Univ. Politehnica din Bucureşti	PhD Supervisor
Prof. Dr. Eng. Liviu GORAS Univ. Tehnica „Gheorge Asachi" Iasi	Referee
CSI. Dr. Adrian DINESCU INCD pt Microtehnologie Bucureşti	Referee
Prof. Dr. Eng. Gheorge BREZEANU Univ. Politehnica din Bucureşti	Referee

BUCUREŞTI 2024

Contents

Thesis objectives and executive summary

After 1965 when the interdigital transducer was discovered, surface acoustic wave (SAW) devices found wide use in applications involving high frequencies, such as: radar pulse compression devices, oscillators, television filters, special radio applications, and more recently satellite and mobile phone communications. SAW and FBAR (film bulk acoustic resonators) filters are used in mobile phones due to their small size, stability and reliability. Usually, non-semiconductor piezoelectric materials are used for their manufacture (quartz, lithium niobate, lithium tantalate, etc.) and they are used on an industrial scale, in particular, due to their very good piezoelectric properties. Also, SAW devices manufactured on these materials are also used for temperature sensors, gas, pressure and humidity sensors due to their high sensitivity and reliability. The first SAW-type structures used to demonstrate the coupling between surface acoustic waves and spin waves were made on the same materials.

The quality of the surface has the effect of making the use of advanced nanolithographic techniques difficult in the manufacture of devices on these materials. For this reason, SAW-type devices made on these materials have a resonance frequency limited to values of the order of 2-2.5 GHz. Modern communication systems (5G, 6G, etc.) involve higher resonant frequencies of SAW devices. Also, a higher resonance frequency is useful for SAW type sensors for various physical parameters, because the sensitivity increases with the resonance frequency, being proportional to its square for mass, humidity and gas sensors and proportional to the resonance frequency for sensors temperature and pressure. In applications related to the coupling of surface acoustic waves with spin waves, a higher resonant frequency (in the 4-10 GHz range) of the SAW device is beneficial because the fundamental resonant frequency of the SAW can be used (and not higher harmonics) for the spin wave coupling.

The limitations of the resonance frequency of SAW devices made on these classic materials, have led in recent years to the development of technologies for making SAWs on thin III-nitrides semiconductor layers with a wide bandgap (GaN, AlN, ScAlN) deposited or grown on semiconductor (silicon, silicon carbide, diamond) or dielectric (sapphire) substrates.

The target of thesis will aim, on the one hand, to develop the technology of SAW devices on materials consisting of III-nitride thin semiconductor layers, (GaN, AlN, ScAlN) deposited/or grown on classic volume semiconductors such as (SiC, Si) and dielectrics (sapphire); on the other hand, the design/simulation, manufacture and characterization of these SAW devices made on these new materials will be followed, for their use as temperature sensors and magnetic sensors. Also, the coupling of surface acoustic waves with spin waves will be analyzed using a SAW structure on ScAlN/Si, the results obtained being spectacular. A special attention was given to simulation

techniques, a field in which the author of this thesis had an important activity even before starting his doctoral studies.

The work is structured in 7 chapters, chapters 2-5 being essentially connected to the new, original results published by me as author/co-author related to this thesis.

The first chapter, the introductory one, is focused on a summary related to elastic waves, the properties of piezoelectric materials, the modes of propagation and the simulation of SAW devices. The Chapters 2, 3 and 4 are dedicated to the simulation and characterization of new temperature sensors based on SAW devices made on various type III materials - nitrides. The 5th Chapter includes the original results related to a magnetic sensor and the realization for the first time of the coupling of surface acoustic waves with spin waves using a SAW structure on $Sc_{0.3}Al_{0.7}N$/Si having a magnetostrictive nickel layer centered in the space between the IDTs. The 6th Chapter presents a synthesis of the original results, publications and my contributions to the publications, and the last chapter, the 7th one - Conclusions, presents the conclusions and future plans.

Chapter 1

Surface acoustic waves devices (SAW)

Short history. The piezoelectric effect was discovery by Curie brothers in 1880, and five years later, Lord Rayleigh demonstrated a propagation of surface acoustic wave and their velocity is smaller than bulk acoustic wave. White and Voltmer's 1965 discovery of the interdigitated transducer deposited on a piezoelectric material which is considered milestone for surface acoustic devices [1].

Elastic waves. The main features of elastic waves are: frequency and ampitude, phase and group velocity, wavelength, displacement and stress, type of wave: transversal or longitudinal [1][2].

Piezoelectric effect. A solid body becomes electrically polarized under the action of a mechanical force (the direct effect) and can be mechanically deformed under the action of an electric field [3].

General properties of III - Nitride semiconductors. Those types of semiconductors are used usually in optoelectronics and high-power electronics [4]. **Aluminium Nitride AlN** it is used microwave application due piezoelectric properties [5]. **Gallium Nitride - GaN** it is one of most studied material from nitrides. **Aluminium nitride dopped with Scandium - ScAlN**. If aluminium nitride is doped with scandium (Sc), the new material (ScAlN) becomes a better piezoelectric material for microelectronics, SAW devices, sensors, etc. [6].

Simulation of SAW devices – Coupling of Modes. A Coupling of Modes it is a method to simulate SAW devices. It is a method which become from optics and it is used to simulate the behaviour of periodic structure. The method is based on three piezoelectric simulations: simulation in short circuit, simulation in open grating, and frequency simulations [7]

Chapter 2

Temperature sensors based on SAW devices on AlN/Si and AlN/glass

2.1 State of the art

Two of the most important advantages of using SAW sensors are: a) their compatibility with the wireless data transmission, and b) the possibility to run without connecting to a voltage source. These advantages are essential while using them in hostile environments [8-10].

III-nitride SAW temperature sensors are compatible with technological processes. It allows one to scale them down and to place them near devices that have to be monitored ('hot spot'). Increasing the resonance frequency lets one to obtain a greater sensor sensibility and to have a more precise temperature assessment. That is why it is useful to develop III-nitride SAW temperature sensors. One of the objectives of this thesis is to develop this kind of sensors, i.e. AlN/Si, AlN/glass, GaN/SiC and GaN/sapphire SAW temperature sensors.

Using an IDT digit/interdigit width of 100-200 nm increases the sensibility [11]. The first SAW temperature sensor with one port was made in 1990 [12]. Its working principle lays on the change of resonance frequency with temperature. In 2003, Palacios makes an analysis of the AlN and GaN sensors advantages and of the materials stability with temperature [13]. Palacios is the first one to introduce these two materials in the development of SAW sensors and makes the first experimental measurements of the frequency temperature coefficient (TCF) for GaN and AlN. In 2010, Ye presents temperature sensors on classical piezoelectric materials [14]. In 2011, Binder introduces a temperature sensor and an integrated system of wireless data transmission [15]. In 2014, A. Müller and our group develops a GaN/Si SAW temperature sensor with more than 5 GHz resonance frequency [16, 17]. In 2015, my colleagues develop a SAW temperature sensor where the Sezawa propagation mode is employed and studied. The first work on an AlN/6H-SiC SAW temperature sensor was published in 2017 by Wang

[19] with an approximate 550 MHz resonance frequency. The next year (2018), our group makes a
SAW temperature sensor on AlN/6H-SiC with the operating frequency in between 3.2 GHz and 5.5 GHz [20]. In 2020, I made and published AlN/Si and AlN/glass SAW temperature sensors. The measurements were made at a temperature in between 6K and 423K [21] (Q2 journal). The sensibilities values were large. Using the modified COM method, the agreement between simulation and experiment gave errors less than 1% on a large range of temperatures. In 2022, I published a first author work with a temperature sensor operating up to 773K using GaN/SiC and GaN/sapphire [22] (Q2 journal). In 2024, I published the work related to a ScAlN/Si temperature sensor [23].

2.2 Measurement and characterization of SAW temperature sensors

The S parameters measurement of SAWs is made with an Anritsu Vector Network Analyzer (VNA MS46122A) together with an on wafer system measurement made bu KarlSüss.

Figure 2.1: Measurement system used in the lab for the temperature sensors

2.3 Temperature SAW sensors based on AlN/Si

The original results presented in this section and the next were published in an IEEE journal (Ultrasonics - Q2) [21]. I am a co-author of this paper.

AlN is a wide band gap semiconductor material. The band gap is of 6eV at room temperature. (111) high-resistivity Silicon has a band gap of 1.12 eV. The thermal conductivity is 149W/mK, being suited for applications where it is used as a substrate for AlN. Borosilicate or glass is an insulator material with the relative dielectric constant of 4.6. I made, simulated and characterized AlN/Si and AlN/glass SAW temperature sensors.

The experiments (which were compared with the simulations) began with the analysis of the metallization influence (material and thickness) on the Rayleigh wave phase velocity in AlN. For the device's metallization, two very popular metals were used: Au and Al. Their thicknesses varied between 25nm and 200nm.

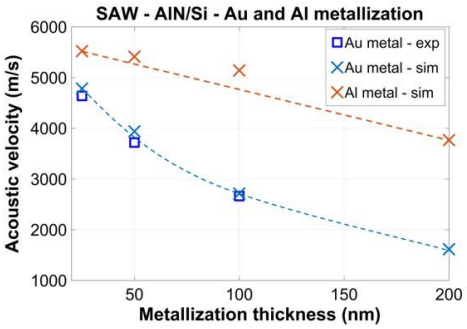

Figure 2.2: Phase velocity with respect to the metallization thickness [21] (@2020 IEEE).

Figure 2.2 presents the values of acoustic velocities calculated from the experiments and simulations for a sample with w=170nm. Different metallization thicknesses are taken into account [21]. As we can see, the velocity decreases as the metallization thickness increases, result useful for the sensors design. For the Au metallization, we observe a completely different behaviour in respect to GaN/Si.

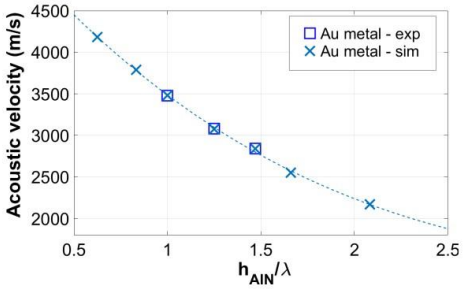

Figure 2.3: Phase velocity with respect to the wavelength [21] (@2020 IEEE).

Figure 2.3 presents experimental and simulated acoustic velocity values for different h_{AlN}/λ at constant metallization thickness. We see in experiments, as well in simulations, that the value of wave phase velocity decreases with the decrease of the wavelength λ [21]. As before, there is a very good agreement between simulation and experiment.

This work was followed by the analysis of these SAW devices in order to see how the frequency varies with the temperature. For the beginning, we show the reflection coefficients S11 (Figure 2.4) for samples with the digit/interdigit width of 170, 200

and 250nm at room temperature [21]. At room temperature the resonance frequencies are: 3.48 GHz for w=250nm, 3.85 GHz for w=200nm and 4.18 GHz for w=170nm [21]. We see that the smallest resonance frequency is for the w=250nm sample, increases for w=200nm and reaches the maximum value for the IDT width of w=170nm [21].

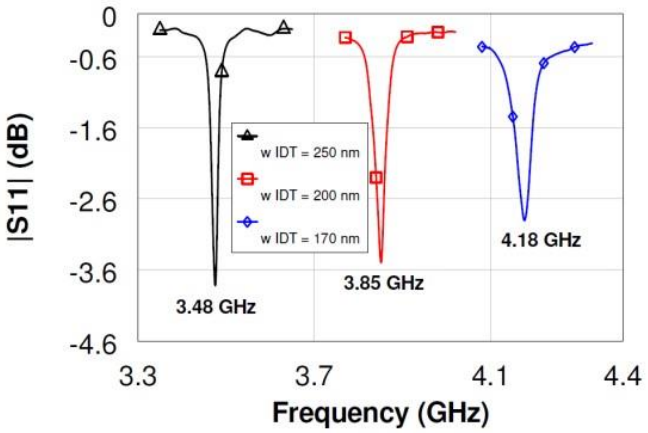

Figure 2.4: S parameters for the three analysed samples [21] (@2020 IEEE).

Figure 2.5 a) presents the resonance frequency change with the temperature in the −268°C÷ +150°C temperature range. We see the sensibility is bigger in the positive temperature range [21]. For temperatures less than −258°C(15K), the resonance frequency decreases with the decrease of temperature and the TCF sign changes [21]. This kind of behaviour was also observed on GaN/Si by our group [11].

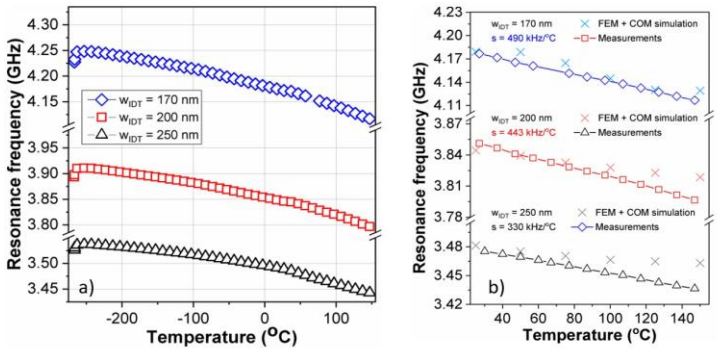

Figure 2.5: Frequency change with the temperature: a) in the range of −268°C → 150°C; b) in the range 0°C÷150° C. Comparison of the experimental values with the simulation ones [21] (@2020 IEEE).

We deduce the sensibility and the TCF from the linear behaviour of the three samples in the 0°C÷ 150°C (Figure 2.5 b). The AlN/Si samples sensibility show high

values for the ones with small wavelength (w=170nm) of 490kHz/°C. The w=200nm shows a value of sensibility of 443kHz/°C, and the last sample a sensibility value of 330kHz/° C. The same behaviour is also seen for the TCF values: 117, 114 and 95 ppm/°C.

We see a good agreement between the experimental data and the FEM+COM simulated data. Figure 2.5 b) shows the comparison between the measurements and simulations. The resonance frequencies obtained as a result of simulations are very close to the experimental ones. The errors depend on the IDT width: for 250nm, we have errors in between 0.12% ÷ 0.77%; for 200nm, the errors are in between 0.04 ÷ 0.57%, and for the last sample w=170nm the errors are in between 0.05 → 0.3% [21].

2.4 Temperature SAW sensors based on AlN/Glass

On a borosilicate (glass) wafer supplied by University Wafer Inc. were made the following SAW devices. The chosen geometrical parameters were: AlN layer thickness: 1µm and the Ti/Au IDTs thickness: 5/95nm. As before, three types of samples were made, with widths of 170nm, 200nm, 250nm and length of 50µm. Figure 2.6 shows the experimental data for the S_{11} parameters for the three samples at room temperature. We can see the resonance frequency increases with the decrease of the width, such as the sample with the digit/interdigit width of 170nm has the biggest frequency.

Figure 2.7 shows the frequency change with the temperature for the three samples. As before, we see that the resonance frequency decreases with the increase of temperature [21]. Once again was confirmed that more compact the samples are, bigger sensibilities and TCFs we find.

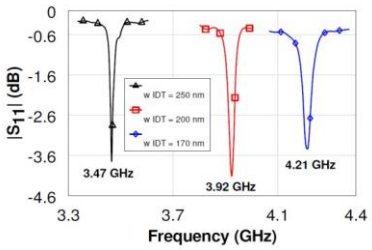

Figure 2.6: S11 parameters at room temperature [21] (@2020 IEEE).

Figure 2.8 shows the resonance frequencies obtained from measurements and simulations in respect to the temperature ($\theta \in (0; \div 150^{o}C)$) for the three samples. We can see an excellent agreement between the experiments and the modified method COM simulations, on a very large range of temperatures (the COM simulation method

was modified by me). One observes the linear resonance frequency behaviour on the $\theta \in (0 \div 150^{o}$ C) temperature range, for the three samples.

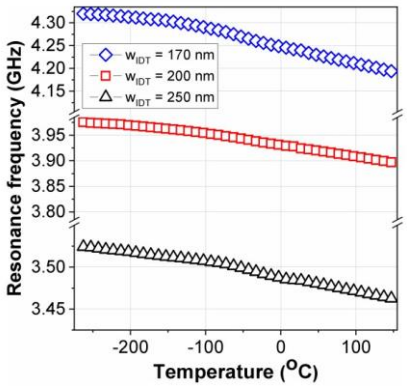

Figure 2.7: The resonance frequency change with the temperature. [21] (@2020 IEEE).

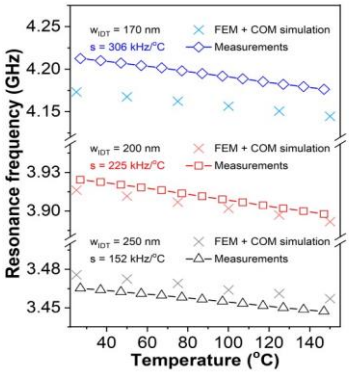

Figure 2.8: The resonance frequency change with the temperature (in the range (0÷150°C)) for the samples made on AlN/glass [21] (@2020 IEEE)

Chapter 3

Temperature sensors based on SAW devices on GaN/SiC and GaN/Sapphire

Silicon carbide is a semiconductor (sapphire is an isolator) with a wide band gap allowing their use as a substrate for GaN SAW temperature sensors up to temperatures of 500°C, and even more. The intrinsic concentration of Silicon ($1.45 \cdot 10^{10}$cm^{-3} at room temperature) makes impossible the use of GaN/Si SAW temperature sensors at

temperatures higher than 200...250ºC. The Silicon becomes intrinsic conductor, even if GaN is a material with a wide band gap.

3.1 Temperature SAW sensors based on GaN/SiC

The original results of this chapter were published in a first author article in the IEEE Access journal [22] (Q2).

The GaN/SiC sensors were made on wafers bought from NTT-AT Japan and have the following geometry: a thickness of 375µm of SiC and a thickness of 0.7µm of piezoelectric GaN containing also a buffer layer of 0.2µm. The latter has the role to accommodate the crystalline network of SiC to GaN [22]. The digit/interdigit width of the IDT was of 400nm, the length of the digits was 50µm; the thickness of the metallization was 80nm (5/75nm Ti/Au) [22]. The IDT was made of 75 pairs of digits, i.e. 150 digits. The sensor also had 50-digit reflectors placed on the left and right of the IDT [22].

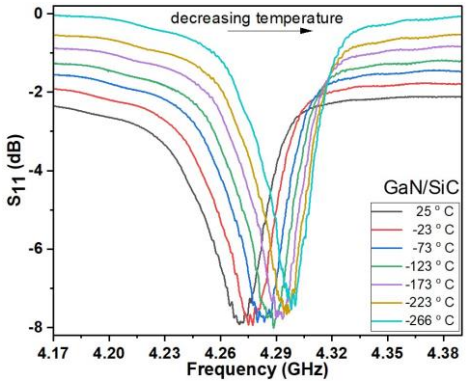

Figure 3.1: S parameters at different temperatures for the GaN/SiC sample [22] (@2022 IEEE).

In Figure 3.1, one sees the response in frequency for the GaN/SiC sample for temperatures in between room temperature and −266ºC. The resonance frequency increases with the temperature decrease [22].

High temperature measurements

High temperature measurements were made at NASA Glenn Research Centre.

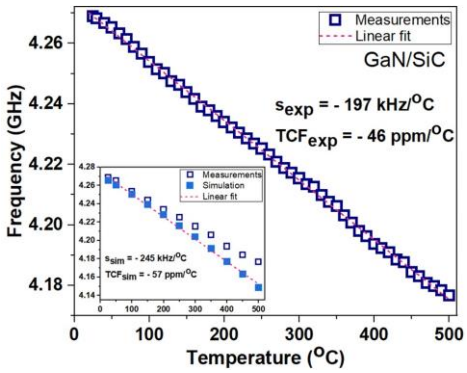

Figure 3.2: The frequency change with the temperature for the GaN/Sic sample. Inset: Comparison between simulation and experiment [22] (@2022 IEEE).

In Figure 3.2, one sees a linear behaviour in the positive temperature range. The same behaviour was also observed in the simulations. The comparison between simulation and measurement is presented in the inset of Figure 3.2. The relative error between experiment and simulation is 0.65% at room temperature, and 3.5% at 500ºC.

3.2 Temperature SAW sensors based on GaN/Sapphire

A new SAW temperature sensor was made and analyzed (measurements and simulations) on a GaN layer on sapphire (GaN/Al2O3). From stability point of view, sapphire is a material allowing measurements at high temperatures. The GaN/sapphire wafer was bought from NTTAT Japan. The fabrication process is similar with the one described in the previous sections.

The wafer geometrical parameters are: the GaN thickness is 1µm and the sapphire thickness is 525±25µm. The geometrical parameters of the sensor are: the Ti/Au metallization thickness is 5/75nm, the IDT digit/interdigit width is 500nm (λ = 2µm) and the length is 50µm.

The temperature measurements were made in the range −266ºC÷25ºC [22].

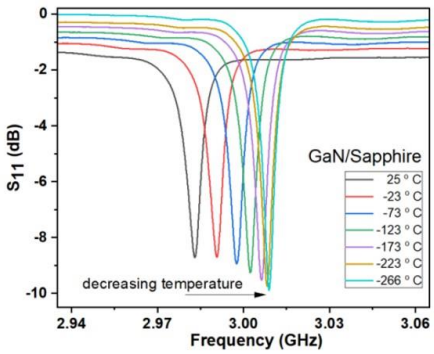

Figure 3.3: S parameters in respect to frequency at different temperatures for the GaN/sapphire sample [22] (@2022 IEEE).

Figure 3.3 presents the S parameters in respect to frequency at different temperatures. Here it is seen too, that the resonance frequency decreases with the temperature increase [22]. The measurements at high temperatures were made at NASA Glenn Research Center.

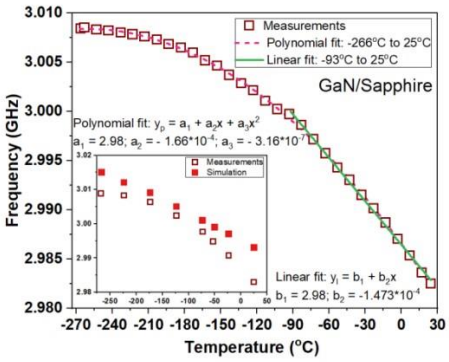

Figure 3.4: The frequency change with the temperature on the negative range of temperatures on the GaN/sapphire sensor [22] (@2022 IEEE).

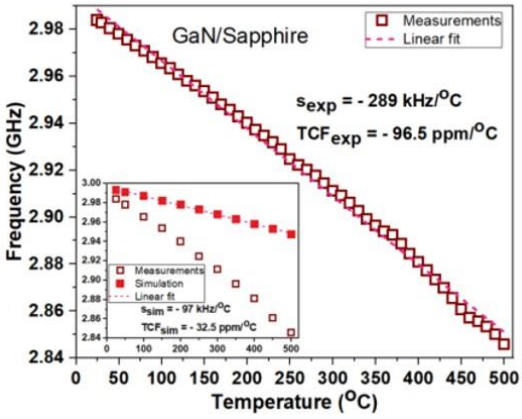

Figure 3.5: The frequency change with the temperature on the positive range of temperatures. Inset: Comparison between simulation and measurements [22] (@2022 IEEE).

Figure 3.5 presents the frequency change with the temperature and the inset presents the comparison between simulations and measurements.

The quality factor Q and the electro-mechanical coupling coefficient k_{eff}^2 ware calculated from the S parameters measurements on the temperature range −266°C÷ 500°C. We obtained for the GaN/SiC devices, at room temperature, 182 and 2.8% for Q and k_{eff}^2, respectively.

For the GaN/sapphire device the quality factor is bigger and has a value of 757, while as the value of k_{eff}^2 is 0.62% [22]. An interesting thing was observed: even if the

resonance frequency is smaller, the GaN/sapphire has the TCF value is bigger than the TCF value of GaN/SiC (−46ppm/ºC).

Chapter 4

Temperature sensors based on SAW devices on ScAlN/Si

The original results from this chapter were published in the prestigious conference proceedings Transducers 2023 and in an IEEJ 2024 article [25] (Q4). I am a co-author of these two publications.

It was observed that if AlN is doped with Sc, the new material ScAlN has superior piezoelectric properties in respect to AlN, and in respect to other III-nitride compounds.

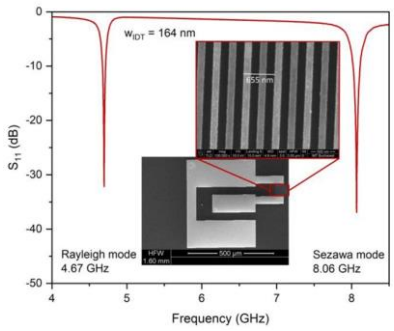

Figure 4.1: S parameter measurement at room temperature and SEM photo of the $Sc_{0.3}Al_{0.7}N$/Si SAW temperature sensor sample

This chapter treats a ScAlN SAW temperature sensor. We wanted to compare the performances (sensibility and TCF) obtained by our group, with the results of other groups on temperature SAW sensors on GaN and AlN. Our group also wanted to do a first all-time analysis concerning the performances of the Sezawa mode on this type of sensor.

The room temperature measurements revealed two resonance frequencies: the Rayleigh mode frequency - 4.69GHz, and the Sezawa mode frequency - 8.06GHz (Figure 4.1). In the same figure, we also see a SEM photo of the sample. From the measurements, we obtain a phase velocity of $Sc_{0.3}Al_{0.7}N$/Si of 3083m/s, much smaller than the phase velocity of sound in Silicon 5200 m/s [24]. As a consequence, the Sezawa mode was to be expected.

Figure 4.2 presents the resonance frequency values for the entire temperature range (from 6K ÷ 430K) and for both propagation modes.

Figure 4.3 presents the experimental and simulated data for a temperature range of most interest (from 0÷150ºC). A very small error of 0.6% is seen between the experimental and simulated data.

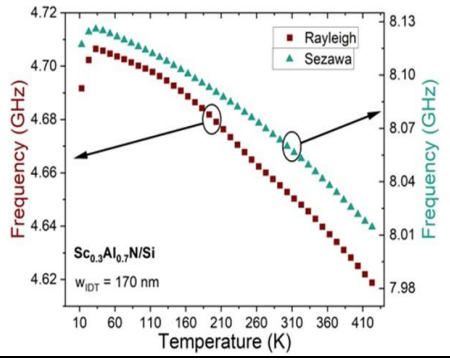

Figure 4.2: The resonance frequency change of the Rayleigh and Sezawa modes in respect to the temperature

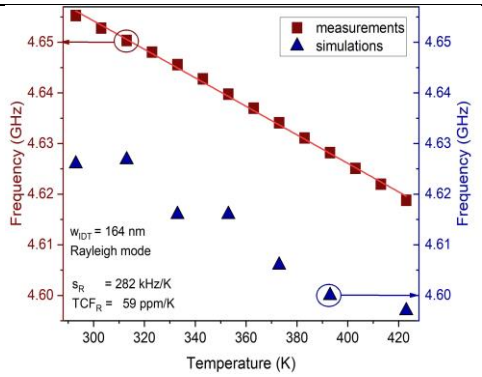

Figure 4.3: The resonance frequency change of the Rayleigh mode in respect to the temperature

In this temperature range, a linear fit can be made. The sensibility of the Rayleigh mode is of 282kHz/K, and the TCF is of 59 ppm/K. For the Sezawa mode, the relative error between the measurements and the simulations The sensibility value is of 383kHz/K and that of the TCF is of 47ppm/K.

Chapter 5

Experimental analysis of magnetic sensors and the coupling of surface acoustic waves with spin waves using SAW devices using III - nitrides compounds

5.1 Generalities

The 5th Chapter of the thesis is dedicated to SAW devices behaviour into the magnetic field. There are analysed two main objectives: the first one is about the experimental analysis of the resonance frequency variation in magnetic field, and the experimental processes of making and characterization of an SAW sensor type; the second one (which is the main one) is about to investigate the coupler between the acoustic and spin waves, which are collective excitations of the magnetic moments.

The interaction between the spin and acoustic waves through magnetoelasticity, was for the first time proposed by Kittel in the 1950 [26], which demonstrated from theoretically point of view the coupler between the acoustic and spin waves. The coupler is obtained when the resonance frequencies of the SAW and spin waves are equal (the last one being very close to the ferromagnetic resonance frequency -FMR), and, the wave vector, k, of both of them, is also, equal [26][27]. Spin waves generation in the region of FMR frequency, using the acoustic waves, or, the generation of the acoustic waves using the spin waves with a magnetic RF field was studied from theoretically point of view in the last decades [27]. In the last 10-15 years, this subject was studied a lot, since it was proved to have applications in the field of data storage, spintronics and magnonics, so that the interest in this field increased [27][28].

5.2 Magnetic SAW sensor based on $Sc_{0.3}Al_{0.7}N$/Si

The work presented here is about how to make a magnetic sensor SAW type on $Sc_{0.3}Al_{0.7}N$/Si. The structure is using only one port, being analysed the resonance frequency variation with the magnetic field, using S11 parameter. The interdigitated transducer is metalized through an magnetostrictive material type (Ni); in this way, the magnetic field will induce the mechanic stress directly to the $Sc_{0.3}Al_{0.7}N$ layer. The thickness of the Si layer is 525 μm, the one of $Sc_{0.3}Al_{0.7}N$ (piezoelectric) layer is 0,8 μm, and the metallic layer thickness (formed between Ni/Au) is 45nm/5nm. Gold is aiming to protect nickel of being oxidized. In this way, the loss of the ferromagnetic properties of Ni is avoided.

The IDTs'width is of 140 nm, which corresponds to a wavelength of device of 560 nm. The total number of digitated electrodes is 150.

The magnetic field measurements were made using the Janis crystal, which was also used for measurements at different temperatures, the magnet is EM 4V with 643 Power Supply from the LakeShore, with a maximum of magnetic field of 460 mT.

The Janis crystal is placed between the two pols of the magnets [29].

The S_{11} parameters were measured at room temperature and also, at150 and 100 K, by changing the magnetic field between −300 mT an +300 mT with an stepf of 0,7 mT.

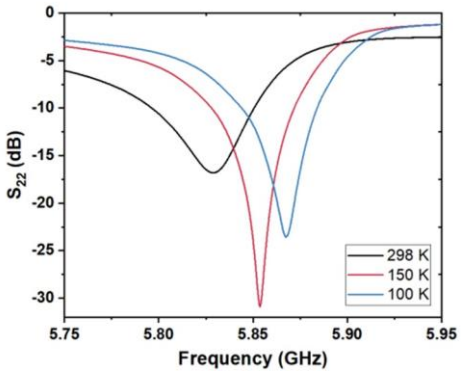

Figure 5.1: S_{11} data over the frequency for each temperature used [29] (@IEEE 2022)

In figure 5.1 there are showed the values for S_{11} and the ones for the zero magnetic field, for the temperatures of 298, 150 and 100 K. All these are considered as references for each temperature, when the magnetic field is applied.

By using the values from the magnetic field and the reference ones, it was calculated the $\Delta f/f_0$ sensitivity, by using the formula:

$$\frac{\Delta f}{f_0} = \frac{f_r(B) - f_r(B=0)}{f_r(B=0)} \tag{5.1}$$

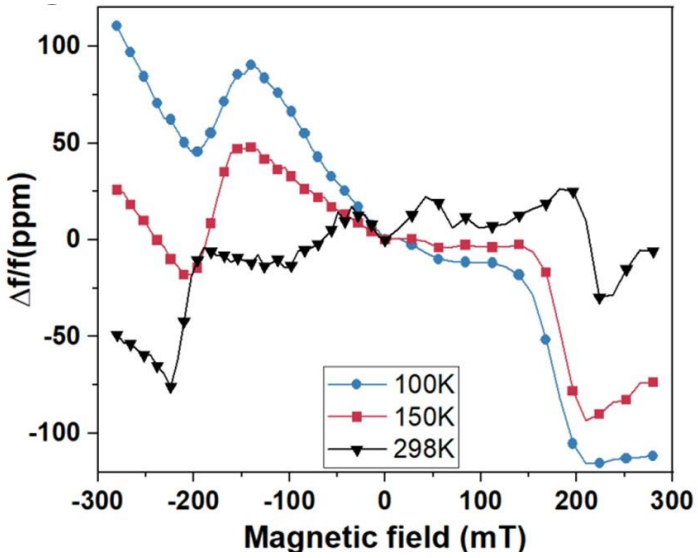

Figure 5.2: $\Delta f/f_0$ function of the magnetic field values in the case of using each temperature value [29](@IEEE 2022)

If we look at the positive axis of the magnetic field, we can see an increased value of the $\Delta f/f_0$ when using 100 K (blue) over 100 ppm, at 150 K (in red) we have 90 ppm, and for room temperature (black), we have the lowest one, 25 ppm. The maximum

point from the negative axe it corresponds to an angle of 45°, between the applied magnetic field and the ones of Ni' IDT [29].

In figure 5.3 it is calculated the normalized sensitivity (ppm/mT) with this formula:

$$S = \frac{1}{f_0}\frac{df}{dB} \tag{5.2}$$

From the figure 5.3, it can be seen that the sensitivity 'behaviour is linear for magnetic field between −300mT and -200 mT, while for +100mT si +300 mT is decreasing.

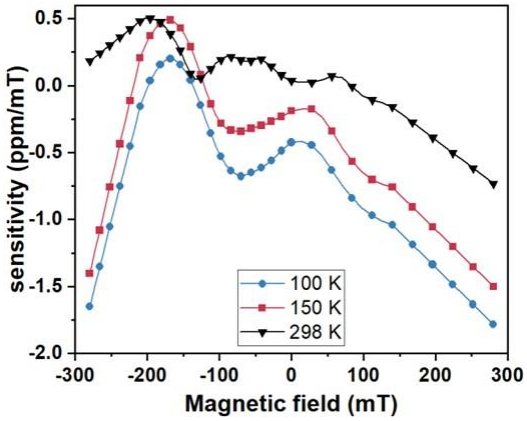

Figure 5.3: Sensitivity variation as function of magnetic field [29] (@IEEE 2022)

For the first time, it was analysed the influence of magnetic field over the resonance frequency, using an ScAlN/Si type device, with Ni made IDT electrodes, being measured S type parameters at low temperatures. The results were presented and published to the IEEE CAS 2022, which I am the main author.

5.3 The interaction of surface acoustic waves with spin waves realized with SAW devices based on $Sc_{0.3}Al_{0.7}N$/Si having magneto strictive nickel layer between IDTs

The interest in the topic of the coupling between the acoustic and the spin waves has grown enormously in the last 10-15 years, which led to the appearance of the first experimental results related to this topic. As in the case of other applications of SAW devices, and in this case the first results appeared on lithium niobate although there is no correlation between the resonance frequency of the SAWs made on this material and the last ferromagnetic resonance being included in the GHz range for the usual magnetostrictive materials.

In all the experiments in the literature performed using lithium niobate and tantalate to highlight the SAW/SW coupling, due to the large difference between the Rayleigh resonance frequency of the SAW and the FMR, it is necessary to use higher harmonics of the SAW which have the disadvantage of a smaller amplitudes, with negative effects on the SAW/SW coupling.

This (sub)chapter of the thesis presents a SAW device with two ports made for the first time on a thin layer of type III-nitride semiconductor deposited on high resistivity silicon (ScAlN/Si), intended for the coupling between the surface acoustic waves and the spin ones. The coupling is realized by means of the nickel magnetostrictive layer placed between the IDTs of the SAW device. The results of two published papers are presented.

$Sc_{0.3}Al_{0.7}N$/Si wafers were used in the technological flow, and the used silicon substrate was of high resistivity. The thicknesses of the piezoelectric and silicon materials were of 0.8 and 526 µm, respectively. The IDTs are composed of 75 pairs of digits and 50 reflectors placed to the left and right of the IDTs. From the geometric point of view, the width of an IDT is 0.17 µm, which corresponds to a wavelength of 0.68 µm. The metallization thickness of the IDTs is 5/45 nm, (Ti/Au) and they were manufactured by electron beam lithography. The distance between the two IDTs is of 200 µm. Between the two IDTs, a 12 nm thick ferromagnetic layer of nickel covered with a very thin layer of gold (3 nm) was deposited in order to protect the nickel layer to be oxidated, an unwanted process that would lead to the loss of its ferromagnetic properties. The ferromagnetic layer has dimensions of 140 × 166 µm [30][31].

An SEM photograph of the experimental structure with the nanolithography process' details is presented in figure 5.4.

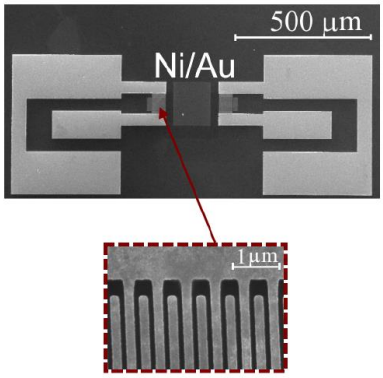

Figure 5.4 SEM photo of the SAW structure, having two ports in order to highlight the coupler [30] (@IEEE2022)

The SAW structures were cut, then into chips and glued on a base (figure 5.5 a)) that can be rotated, so that to measure the transmission parameters (S12, S21), in a magnetic field at different angles between the direction of the applied magnetic field and the velocity vector of the surface acoustic wave. Figure 5.5 b) shows the especially homemade device in the laboratory, which allows the measurement of S parameters.

In figure 5.5 c), the Janis cryostat that also contains the custom device (figure 5.5 b) is placed between the poles of an EM 4V 643 Power Supply electromagnet from

LakeShore. The maximum magnetic field that can be obtained at the level of the device (considering that the cryostat is placed between the poles of the electromagnet) is of 420 mT.

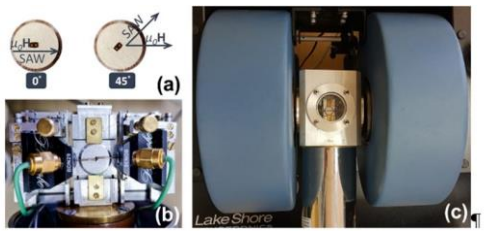

Figure 5.5: The circular angle required to rotate the structures at various angles (a); the specially built device in the laboratory capable of measuring parameters S (b); the Yanis cryostat and the poles of the LakeShore magnet [30] (@IEEE2022)

The figure 5.6 a) shows S11 parameters for this device, in a zero magnetic field, and the appearance of two resonances can be observed: Rayleigh at 4.67 GHz and Sezawa at 8.05 GHz. It is also observed that the amplitude of the signal in the case of Sezawa is much higher than that of Rayleigh. Transmission parameters for the Rayleigh and Sezawa mode are presented in figure 5.6 a) [30].

A measure of the coupling between the acoustic and spin waves consists in the absorption of energy from the acoustic waves, observable by the decrease of S21, S12 (transmission parameters), at resonance, obviously in the magnetic field. The measurements are made at frequencies in the vicinity of the resonances (circled areas in figure 5.6 b)) [30].

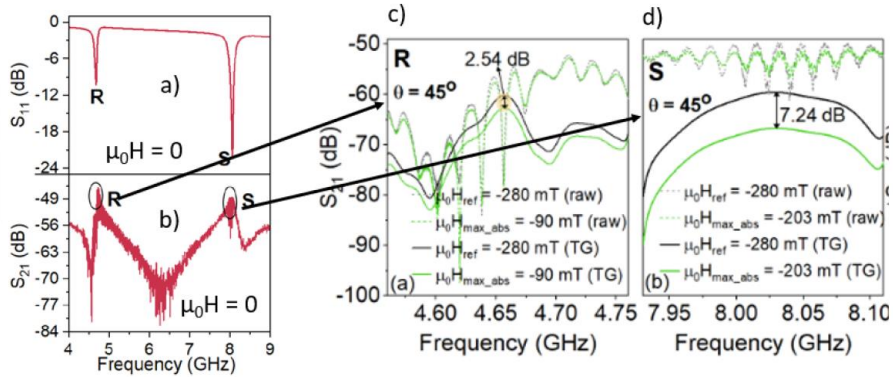

Figure 5.6: S21 values measured at the reference value of μ0Href (broken black curve) and at $\mu_0 H_{max\_abs}$, the value at which the maximum absorption was observed (broken green curve) for Rayleigh (left) and Sezawa -right ("raw" measurements); TDR measurements (green and black continuous lines) [30] (@IEEE2022)

The maximum coupling between the surface and spin acoustic waves occurs where the amplitude of S21 decreases the most. In figure 5.6 c) and d) the measurements

performed in the magnetic field at θ = 45◦ are detailed, for the two modes, Rayleigh and Sezawa, respectively. These measurements were made according to the rigors of magnetic measurements, considering as a reference value the minimum value of the field at which the measurements started (-280 mT) ¸and not the value B=0 [30].

In this figure, one can observe the decrease of S21 around the resonance value B= -90 mT - dotted green curve, compared with the dotted black curve corresponding to the reference value of -280 mT, for the Rayleigh mode [30].

Similarly, in figure 5.6 d) one can observe the decrease of S21 around the resonance value B=-203 mT - dotted green curve, compared with the dotted black curve corresponding to the reference value of -280 mT, for the Sezawa mode [30].

These determinations refer to the raw values of S21 values. It is obvious, visually, the decrease (even from the raw measurements); this decrease is more pronounced for the Sezawa mode.

For this kind of measurements, more precise determinations are needed, consisting of "time gated determinations" obtained by "time domain reflectometry" with the role of eliminating parasitic electromagnetic signals. The results of these determinations are presented in figure 5.6 c) and d). It is about the continuous green curves for the resonance fields, compared to the continuous black curves related to the reference field. With their help, we can appreciate a decrease in the signal by 2.54 dB for the Rayleigh mode and 7.24 dB for the Sezawa mode, particularly spectacular results; for the Sezawa mode, these were highlighted for the first time [30].

The maximum coupling between surface and spin acoustic waves occurs where the amplitude of S21 decreases the most. Figures 5.7 show the measured values for S21 as a function of frequency at an angle of 45◦ for both modes. Thus, in figure 5.7 a) we have the values of S21 for the Rayleigh mode when the magnetic field is 280 mT (reference) and for the value of −90 mT, where the highest absorption was observed. The figure 5.7 b) presents the Sezawa case and the −203 mT wave value of the magnetic field where the highest absorption occurs. It is also possible to observe the decrease of the signal by 2.54 dB for Rayleigh and 7.24 dB for Sezawa [30].

To measure the energy transfer from the acoustic to the magnetic domain, the difference is made between S21 for each magnetic field and the reference S21 measured at the magnetic field value of μ0Href = −280 mT:

$$\Delta S_{21} = \left| S_{21}^{\mu_0 H_n} - S_{21}^{\mu_0 H_{ref}} \right| . \tag{5.3}$$

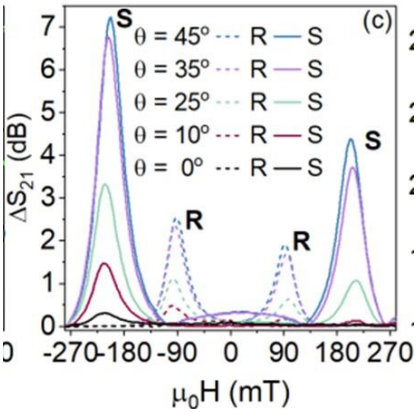

Figure 5.8: Energy transfer ΔS21 for the entire magnetic field range and the 5 chosen angles (@IEEE2022)

Figure 5.8 shows the ΔS21 values for all angles and for the two resonance frequencies. It can be seen that the maximum effect occurs at both resonances and is greater for the Sezawa case and at the 45 angles [30].

A 4 times greater decrease in amplitude can be observed for the Sezawa mode when the value of the magnetic field is 203 mT, for an angle of 45◦. For the Rayleigh mode, a 2-fold decrease in amplitude occurs at a magnetic field of 90 mT [30]. The absorption values are very high for the Rayleigh waves, in our opinion comparable to the best results obtained so far (reported as we have shown only on classical piezoelectric substrates). The Sezawa mode absorption values represent, however, the "state of the art" being substantially higher than what has been reported up to now, it is true only for the Rayleigh mode because the works reported so far could not benefit from the non-existent Sezawa mode on "nonlayered structures" [30]. We consider that the results reported here are the best results regarding energy transfer from SAW waves to spin waves up to the time of publication.

I was co-author of the papers published on this topic, a paper in the journal IEEE Electron Device Letters and a paper at the conference IEEE CAS 2021.

Chapter 6

Contributions to the progress of the field, published works, original contributions, personal participation in works published within the collective of authors

The topic of this thesis is, on the one hand, the development of SAW device technology on materials made of thin semiconductor layers of type III- rivets,

(GaN, AlN, ScAlN) deposited/or grown on classic volume semiconductors such as (SiC, Si) or dielectrics (sapphire).

Having a global topic, with the use of advanced technologies, under the conditions of the integration of the collective in international collaborations, within European research programs, new, interesting, original results could be obtained, some even representing the current state of the art, as well as making publications in prestigious journals.

The papers published during doctoral school and whose topic is analysed in the thesis:

A. ISI Journals (R)

R1: Nicoloiu, Alexandra, George E. Stan, Claudia Nastase, **George Boldeiu**, Cristina Besleaga, Adrian Dinescu, and Alexandru Müller. *"The Behavior of Gold Metallized AlN/Si- And AlN/Glass-Based SAW Structures as Temperature Sensors."* IEEE Transactions on Ultrasonics, Ferroelectrics, and Frequency Control 68(5):1938–48. 2021.**(Q2)**

R2: Boldeiu George, George E. Ponchak, Alexandra Nicoloiu, Claudia Nastase, Ioana Zdru, Adrian Dinescu, and Alexandru Müller. *"Investigation of Temperature Sensing Capabilities of GaN/SiC and GaN/Sapphire Surface Acoustic Wave Devices."* IEEE Access 10:741–52.
2022 .**(Q2)**

R3: Zdru, I., C. Nastase, L. N. Hess, F. Ciubotaru, A. Nicoloiu, D. Vasilache, M. Dekkers, M. Geilen, C. Ciornei, **G. Boldeiu**, A. Dinescu, C. Adelmann, M. Weiler, P. Pirro, and A. Müller. *"A GHz Operating CMOS Compatible ScAlN Based SAW Resonator Used for Surface Acoustic Waves/Spin Waves Coupling."* IEEE Electron Device Letters 43(9):1551–54. 2022.**(Q1)**

R4: Alexandra Nicoloiu, **George Boldeiu**, Claudia Nastase, Monica Nedelcu, Cristina Ciornei, Ioana Zdru, George Stavrinidis, Dan Vasilache, Antonis Stavrinidis, Adrian Dinescu, George Konstantinidis, Alexandru

R5: Pati Tripathi, S., Bonen, S., Bharadwaj, A., Jager, T., Nastase, C., Iordanescu, S., **Boldeiu, G**., Pa¸steanu, M., Nicoloiu, A., Zdru, I., Mller, A., & Voinigescu, S. P. (2022). "Characterization and Modeling of Quantum Dot Behavior in FDSOI Devices". IEEE Journal of the Electron Devices Society, 10. (Q2) https://doi.org/10.1109/JEDS.2022.3176205

R6: Aldrigo, M., Dragoman, M., Iordanescu, S., **Boldeiu, G**., Crippa, P., Biagetti, G., Turchetti, C., Pierantoni, L., Mencarelli, D., Xavier, S.,

Gangloff, L., & Ziaei, A. (2022). ”Tunable and Miniaturized Micro Variable Capacitors”. IEEE Transactions on Nanotechnology, 21, 118–130. https://doi.org/10.1109/TNANO.2022.315wave3561 Filters Using Carbon Nanotube-Based (Q2). Müller, *“Experimental analysis of Rayleigh and Sezawa modes resonance frequencies in SAW devices manufactured on Sc0.3Al0.7N/Si”*, IEEJ Transactions on Electrical and Electronic Engineering Japan, 2024 **(Q4)**

B. Conferinte (C) cotate ISI

C1: Alexandra Nicoloiu, **George Boldeiu**, Claudia Nastase, Monica Nedelcu, Cristina Ciornei, Ioana Zdru, George Stavrinidis, Dan Vasilache, Antonis Stavrinidis, Adrian Dinescu, George Konstantinidis and Alexandru Müller *“Temperature Behaviour of Rayleigh, Sezawa and Lamb Mode Resonance Frequencies of 30% ScAlN/Si SAW Devices”*, pp. 1608-1611, Transducers 2023 Kyoto, JAPAN, 25 - 29 June 2023

C2: Boldeiu, G., C. Nastase, A. Nicoloiu, A. Florescu, I. Zdru, D. Vasilache, A. Dinescu, and A. Müller. 2022. *“Resonance Frequency vs. Magnetic Field Analysis for ScA1N/Si SAW Resonators with Magnetostrictive Metalization on the Nanolithographic IDTs.”* in Proceedings of the International Semiconductor Conference, CAS. Vols. 2022-October.

C3: Vasilache, D., A. Nicoloiu, **Boldeiu, G**, I. Zdru, T. Kostopoulos, M. Nedelcu, A. Stavrinidis, C. Nastase, G. Stavrinidis, G. Konstantinidis, A. Dinescu, and A. Müller. 2022. *“Development of High Frequency SAW Devices Devoted for Pressure Sensing.”* in Proceedings of the International Semiconductor Conference, CAS. Vols. 2022-October.

C4: Nicoloiu, A., C. Nastase, I. Zdru, D. Vasilache, **G. Boldeiu**, M. C. Ciornei, A. Dinescu, and A. Müller. 2021. *“Novel ScAlN/Si SAWType Devices Targeting Surface Acoustic Wave/Spin Wave Coupling.”*
Proceedings of the International Semiconductor Conference, CAS 2021-October:67–70, 2021

C5: Tripathi, S. P., Bonen, S., Nastase, C., Iordanescu, S., **Boldeiu, G**., Pa¸steanu, M., Muller, A., & Voinigescu, S. P. (2021). “Compact Modelling of 22nm FDSOI CMOS Semiconductor Quantum Dot Cryogenic I-V Characteristics”. ESSCIRC 2021 - IEEE 47th European Solid State Circuits Conference, Proceedings, 43–46, https://doi.org/10.1109/ESSCIRC53450.2021.9567759

C6: Boldeiu, G., Dragoman, M., Aldrigo, M., Iordanescu, S., & Cismaru, A. (2022).” Multi-physics simulations of pyroelectric harvesters based on nanoscale ferroelectrics”. Proceedings of the International Semiconductor Conference, CAS, 2022-October. https://doi.org/10.1109/CAS56377.2022.9934509

Papers R1-R4 and conference papers C1-C4 are directly related to the new and original results reported in the thesis. My contributions to these works detailed in detail in Chapter 6 of the thesis. I am the first author of an article in the IEEE Access magazine (Q2), and two IEEE conference papers.

Chapter 7

Conclusions and perspectives

The paper presents the individual contributions and those belonging to the doctoral student within the collective of which he was a part, in the development of new physical models, new technologies, innovative simulation, design and characterization methods related to the technology of SAW-type devices on thin layers of type III semiconductors- nitrides (AlN, GaN, ScAlN) deposited or grown on volume semiconductors (Si, SiC) or dielectrics (sapphire).

The main activities, achievements and results of the work are presented in chapters 2-5. These chapters also follow the main publications that the author of the thesis signed as the main author or co-author.

Below we present the conclusions of these achievements and results.

Chapter 2 – Temperature sensors based on SAW devices made of AlN/Si and AlN/glass

The published work on which this chapter is based [**R1 chap 6, Q2**] is one the first articles that analyse the behaviour of SAW-type structures made on thin layers of AlN deposited on various bulk semiconductor substrates. AlN/Si structures are for the first time used as temperature sensors according to the authors' knowledge (results were also published on AlN/diamond and AlN/SiC - much more expensive materials as a substrate with more difficult technologies). The SAW structures on AlN/Si proved excellent performance as temperature sensors: for sensitivity and temperature coefficient of frequency (TCF) the values were higher than those obtained by the same authors for SAW structures on GaN/Si and for AlN/glass.

For the first time, the modified FEM+COM method was used to simulate the behaviour of the structures; COMSOL MultiPhysics was used for FEM

simulation. This simulation represents an important step in extracting the COM parameters for all considered temperatures. The experimental values were compared with the simulated ones, resulting in very small error values (lower than those reported in the literature).

Chapter 3 – Temperature sensors based on SAW devices made of GaN/SiC and GaN/sapphire

The published work related to this chapter [**R2 chap 6, Q2**] published in 2022 in IEEE Access, of which I am the first author, represents a collaboration between IMT and NASA in the realization and characterization of functional SAW sensors over a very large temperature range, from cryogenic temperatures (a few degrees K) to temperatures higher than 500◦C. Here the behaviour of single-port resonator structures made on GaN/SiC and GaN/sapphire was presented.
The SiC and sapphire substrates ensure, together with the GaN "over-layer", operation at high temperatures (silicon becomes intrinsically - therefore conductive at temperatures higher than about 200◦ C). Technology, design, simulation and measurements at low temperatures were done at IMT, while the microwave measurements of the variation of resonance frequency with temperature at high temperatures (150 − 500◦C) were made at NASA. The elements of originality in design, simulation, technology and measurements are evident. For the first time, from the measurements of parameters S, the values of the quality factor Q and the electromechanical coupling coefficient (k2 eff) were calculated for the entire temperature range (−266◦C ÷500◦C).
It was observed that the device made on GaN/sapphire has a higher TCF value (−96.5 ppm/◦C) compared to the value of the GaN/SiC device (−46 ppm/◦C).

Chapter 4 – Temperature sensors based on SAW devices made of ScAlN/Si

There were described two papers in this chapter: one published in the Proceedings of the prestigious conference Transducers 2023, (**C1, chapter 6**), and, the second one, published in the Japanese magazine "IEEJ Transactions on Electrical and Electronic Engineering" (**R4, chapter 6 Q4**) in 2024, at both being co-author.

This chapter presents the first SAW devices made on ScAlN/Si intended as temperature sensors. The determinations of the sensitivity and the temperature coefficients of the frequency were determined in a vacuumed enclosure so that the measurements could not be vitiated by the adsorption of atmospheric gases. Thus, it was demonstrated that the TCF values for the Rayleigh and Sezawa modes are higher enough to ensure better performance than for GaN/Si. Moreover, the results obtained could be compared with those reported by another (only) published work on this new topic, for the Rayleigh mode.

The sensitivity and the TCF were determined for both highlighted modes. In the case of Sezawa TCF mode, to the authors' knowledge, such a thing it is reported for the first time. The simulations of the resonance frequency’ variation with temperature is in good agreement with the experiment.

Chapter 5

Subchapter - 5.2 The SAW magnetic sensor made of $Sc_{0.3}Al_{0.7}N$/Si

This subchapter describes the technology of a magnetic sensor on ScAlN, which was presented and published at the CAS 2022 conference (C2 chapter 6) where I am the first author. It was described for the first time the magnetic sensor made on ScAlN/Si. Following this idea, the same team, made, two years earlier, the first magnetic sensor on GaN/Si. The results are particularly promising; the original design of the magnetic sensor and the magnetic measurements made for the first time at cryogenic temperatures with such a sensor are presented.

Subchapter - 5.3 The interaction of acoustic waves from the surface on $Sc_{0.3}Al_{0.7}N$/Si with the spin waves made of an thin magnetoresistive Ni layer

Subchapter 5.3 is based on a paper published in IEEE Trans. On Electron Devices Lett (**R3 chapter 6, Q1**), of which I am the author and we consider it to represents a "breakthrough" in research in the field, being the first paper that experimentally presents the coupling of surface acoustic waves with spin waves using thin semiconductor layers, (in this case on Sc0.3Al0.7N/Si, the newest, exotic and promising type III-nitride materials).

This subchapter is based on a paper published in IEEE Trans. On Electron Devices Lett (**R3 chapter 6, Q1**), of which I am the author and we consider it to have represented a "breakthrough" in research in the field, being the first paper that experimentally presents the coupling of surface acoustic waves with spin waves using thin semiconductor layers, (in this case on Sc0.3Al0.7N/Si, the newest, exotic and promising type III-nitride materials). Both, the Rayleigh and the Sezawa propagation mode are analyzed. For the Rayleigh mode (at about 5 GHz), the fraction of energy transferred from surface acoustic to spin waves represents 50% for a field of 90 mT, a value comparable to the best reported ones. In the case of the Sezawa mode, the fraction of energy transferred from surface acoustic to spin waves is much higher than the fractions reported up to the time of publication. Previous reports related to this topic are exclusively on volume piezoelectric materials (lithium niobate), Rayleigh mode. On SAW structures made on "layered structures", the Sezawa mode can appear, under certain conditions, as in our case. Thus, for a thin Ni film (15 nm) placed between the IDTs of a SAW device made on Sc0.3Al0.7N/Si, the transmission parameters were adjusted in amplitude, in relation to both the size and the orientation of the magnetic field, thus that a 4-fold decrease in amplitude was measured for the Sezawa mode, at a frequency of about 8 GHz, at a magnetic field of 203 mT and an angle of 45 degrees between the magnetic field and the propagation direction of the SAW device.

We also published partial results at the IEEE conference, CAS 2022 (C4, chap. 6).

Perspectives

Many of the reported results have a high degree of novelty and lead to optimistic conclusions regarding the future of these devices. The research related to the coupling of SAW waves with spin waves for various geometries of the magnetostrictive layer and various thicknesses of the ScAlN layer must be deepened, with the premise of even more spectacular results than those reported by our group. Other types of sensors based on III-nitride compounds (stain, stress, humidity gas) should also be addressed, with the prospect of better results in terms of sensitivity.

Finally, we consider that SAW filters on ScAlN should be addressed in our group. The material is still in the research stage, the production technology is not mature enough, but we believe that the high values of k2eff and Q obtained for this material compared to those obtained for GaN and AlN will ensure a future in SAW devices for the filters used in "beyond 5 G" communication systems.

Many of the reported results have a higher degree of novelty and lead to optimistic conclusions regarding the future of these devices. The research related to the coupling of SAW waves with spin waves for various geometries of the magnetostrictive layer and various thicknesses of the ScAlN layer must be deepened, with the premise of even more spectacular results than those reported by our group. Other types of sensors based on III-nitride compounds (stain, stress, humidity gas) should also be addressed, with the prospect of better results in terms of sensitivity.

Bibliography

[1] Royer, D. and Dieulesaint, E. *Elastic Waves in Solids I*, volume I. (2000).

[2] Cheeke, J. D. N. *Fundamentals and applications of ultrasonic waves*. CRC Press, (2012).

[3] Tichy´, J., Erhart, J., Kittinger, E., and P˘r´ıvratsk´a, J. *Fundamentals of Piezoelectric Sensorics: Mechanical, Dielectric, and Thermodynamical Properties of Piezoelectric Materials* , 1–207 (2010).

[4] Hua, Q., Ma, B., and Hu, W. *Encyclopedia of Materials: Technical Ceramics and Glasses* **3-3**, 74–83 1 (2021).

[5] Bhugra, H. and Piazza, G., editors. *Piezoelectric MEMS Resonators*. Springer International Publishing, (2017).

[6] Bespalova, K., Osterlund, E., Ross, G., Paulasto-Kr¨ockel, M., Sebastian,¨ A. T., Karuthedath, C. B., Mertin, S., and Pensala, T. *Journal of Microelectromechanical Systems* **30**(2), 290–298 (2021).

[7] Plessky, V. *International Journal of High Speed Electronics and Systems* **10**, 867–947 12 (2000).

[8] Lewis, M. *IEEE Ultrasonics Symposium, 2005.* **2**, 800–809 (2005).

[9] Borrero *et al.*, G. *Sensors and Actuators A: Physical* **203**, 204–214 (2013).

[10] Stevens *et al.*, D. In *Fourth International Symposium on Acoustic Wave Devices for Future Mobile Communication Systems, Chiba University, Japan*, (2010).

[11] Müller *et al.*, A. *Sensors and Actuators A: Physical* **209**, 115–123 (2014).

[12] Viens, M. and Cheeke, J. N. *Sensors and Actuators A: Physical* **24**(3), 209– 211 (1990).

[13] Palacios *et al.*, T. *Proceedings of the IEEE Ultrasonics Symposium* **1**, 57–60 (2002).

[14] Ye *et al.*, X. , 585–588 (2010).

[15] Binder, A. and Fachberger, R. *IEEE Sensors Journal* **11**(4), 966–970 (2011).

[16] Müller *et al.*, A. Institute of Electrical and Electronics Engineers Inc., (2014).

[17] Müller *et al.*, A. In *2014 IEEE MTT-S International Microwave Symposium (IMS2014)*, 1–4, (2014).

[18] Müller *et al.*, A. *IEEE Electron Device Letters* **36**, 1299–1302 (2015).

[19] Wang *et al.*, W. Z. In *2017 19th International Conference on Solid-State Sensors, Actuators and Microsystems (TRANSDUCERS)*, 942–945, (2017).

[20] Nicoloiu *et al.*, A. volume 2018-Octob, (2018).

[21] Nicoloiu *et al.*, A. *IEEE Transactions on Ultrasonics, Ferroelectrics, and Frequency Control* (2020).

[22] Boldeiu *et al.*, G. *IEEE Access* **10**, 741–752 (2022).

[23] Nicoloiu *et al.*, A. In *The 22nd International Conference on Solid-State Sensors, Actuators and Microsystems Kyoto, Japan*, (2023).

[24] Institute, I. (1918). Accessed on 20 11, 2023.

[25] Nicoloiu, A. et al. *IEEJ Transactions on Electrical and Electronic Engineering*, (2024)

[26] Kittel, C. *Phys. Rev.* **73**, 155–161 Jan (1948).

[27] Delsing *et al.*, P. *Journal of Physics D: Applied Physics* **52**(35), 353001 jul (2019).

[28] Munteannu, I. *Fizica Solidului*, volume I. (2003).

[29] Boldeiu *et al.*, G. In *2022 International Semiconductor Conference (CAS)*, 187–190. IEEE, (2022).

[30] Zdru *et al.*, I. *IEEE Electron Device Letters* **43**(9), 1551–1554 (2022).

[31] Nicoloiu *et al.*, A. In *2021 International Semiconductor Conference (CAS)*, 67–70, (2021).